# Role of Ge in Bridging Ferromagnetism in the Giant Magnetocaloric Gd$_5$(Ge$_{1-x}$Si$_x$)$_4$ Alloys

D. Haskel,[1] Y. B. Lee,[2] B. N. Harmon,[2] Z. Islam,[1] J. C. Lang,[1] G. Srajer,[1] Ya. Mudryk,[2]
K. A. Gschneidner, Jr.,[3] and V. K. Pecharsky[3]

[1]*Advanced Photon Source, Argonne National Laboratory, Argonne, Illinois 60439, USA*
[2]*Condensed Matter Physics Program, Ames Laboratory, Iowa State University, Ames, Iowa 50011-3020, USA*
[3]*Ames Laboratory and Department of Materials Science and Engineering, Iowa State University, Ames, Iowa 50011-3020, USA*
(Received 10 October 2006; published 15 June 2007)

X-ray magnetic circular dichroism (XMCD) measurements and density functional theory (DFT) are used to study the electronic conduction states in Gd$_5$(Ge$_{1-x}$Si$_x$)$_4$ materials through the first-order bond-breaking magnetostructural transition responsible for their giant magnetocaloric effect. Spin-dependent hybridization between Ge $4p$ and Gd $5d$ conduction states, which XMCD senses through the induced magnetic polarization in Ge ions, enables long-range Ruderman-Kittel-Kasuya-Yosida ferromagnetic interactions between Gd $4f$ moments in adjacent Gd slabs connected by Ge(Si) bonds. These interactions are strong below but weaken above the Ge(Si) bond-breaking transition that destroys 3D ferromagnetic order.

The family of giant magnetocaloric Gd$_5$(Ge$_{1-x}$Si$_x$)$_4$ materials continues to attract considerable attention due to its unusual magnetic properties and its potential for use in magnetic refrigeration near room temperature [1–9]. Unlike adiabatic demagnetization of paramagnetic substances, where refrigeration is achieved by harnessing changes in magnetic entropy alone, these materials display a concomitant magnetostructural transition resulting in comparable structural and magnetic entropy contributions to the magnetocaloric effect [8]. The coupling with the martensiticlike transition causes the usual second-order paramagnetic (PM) to ferromagnetic (FM) transition to become first order. In addition, a magnetic field applied near the Curie temperature triggers the transition [8]. Both the structural contribution to entropy and the first-order character of the magnetostructural transition lead to a giant magnetocaloric effect where adiabatic temperature changes as high as $\Delta T \approx 16$ K can be obtained in the vicinity of room temperature in applied fields below 5 Tesla [3].

The magnetostructural phase transition involves large shear displacements ($\approx 0.45$ Å) of Gd-containing slabs along the $a$ direction of the orthorhombic unit cell, breaking the Ge(Si) covalent bonds that connect the slabs in the $b$ direction with the concomitant destruction of FM ordering (see Fig. 2 for a schematic view of the structure). It has been hypothesized that the breaking of Ge(Si) bonds between the sheared slabs weakens the magnetic interslab coupling [10]. In this Letter, we test and quantitatively confirm that hypothesis with detailed first principles electronic structure calculations and corresponding element- and orbital-specific x-ray magnetic circular dichroism (XMCD) measurements. We show that a large hybridization between Ge $4p$ orbitals and spin-polarized $5d$ orbitals on Gd leads to a small net magnetization on Ge and a long-range Ruderman-Kittel-Kasuya-Yosida (RKKY) indirect FM exchange coupling [11] between $4f$ Gd moments in adjacent Gd slabs. This coupling is significantly weakened

when the slabs shear at the bond-breaking transition, resulting in destruction of FM order.

Polycrystalline samples used in this work were prepared as described in Ref. [12]. The XMCD measurements were done on fine powder samples embedded in a thermoplastic resin that prevents particle rotation in applied magnetic fields and ensures proper powder averaging (crystal structure [13] and magnetic response [10] are anisotropic). All measurements were done in transmission geometry on warming, with special care taken to account for hysteresis in temperature and field cycles characteristic of the first-order magnetic-martensitic transitions [3]. XMCD measurements at the Ge $K$ ($1s \rightarrow 4p$ transition at 11.103 keV) and Gd $L_3$ ($2p_{3/2} \rightarrow 5d$ transition at 7.243 keV) edges were performed to probe the magnetic polarization of Ge $4p$ and Gd $5d$ states, respectively, through the magnetostructural phase transition. The orbital specificity of XMCD dictated by dipole selection rules [14] provides a direct probe of polarization in the electronic states responsible for the indirect exchange coupling among localized Gd $4f$ moments [11,15]. The XMCD spectra were obtained from measurements of the helicity-dependent absorption as $(\mu^+ - \mu^-)/\Delta\mu_0$, where $\mu^{+,-}$ are absorption coefficients for opposite x-ray helicity and $\Delta\mu_0$ is the absorption edge jump. For these measurements, the polarization of synchrotron radiation from undulator beamline 4-ID-D of the Advanced Photon Source was converted from linear to circular using phase-retarder optics [16]. The dichroism was measured by switching x-ray helicity (12 Hz) at each energy point through the absorption edge and using a lock-in amplifier to detect the modulation in the absorption coefficient at the switching frequency [17]. All measurements were carried out for two directions of the applied magnetic field, along and opposite the incident photon wave vector $\hat{k}_i$, to check for systematic errors in the XMCD signals. XMCD hysteresis loops were used to ensure full reversal of magnetization.

Figure 1 shows XMCD data at the Ge $K$ and Gd $L_3$ edges through the magnetostructural transition of $x = 0.125, 0.5$ samples. Raw data are shown for $x = 0.5$ in Figs. 1(a) and 1(b) although identical XMCD line shapes were obtained for the $x = 0.125$ sample [18]. The integrated XMCD signals normalized to their low-$T$ saturation values are shown in Fig. 1(c). For comparison, SQUID bulk-magnetization data measured on polycrystalline samples ($H = 2$ T) are also shown. The presence of significant Ge $K$-edge XMCD signal indicates that the Ge $4p$ states probed by this electronic transition carry magnetic polarization. The helicity-independent absorption coefficient $\mu = (\mu^+ + \mu^-)/2$, also shown in Fig. 1, shows that these polarized states are located near the Fermi level, i.e., right at the onset of the photoelectric absorption process. The magnitude of the Ge $K$-edge dichroism of $\approx 0.3\%$ is comparable to that measured at the $K$ edges of Fe, Co, and Ni metals [19]. However, as discussed below, the spin polarization of Ge $4p$ states is induced by hybridization with $5d$ states, not from *on-site* exchange as occurs for the $3d$ transition metals (Ge is $3d^{10}$). The induced nature of Ge polarization is consistent with its strong coupling to the Gd polarization: they follow the same temperature dependence and disappear at the FM-PM, bond-breaking magnetostructural transition.

The structural transition is probed by x-ray absorption fine structure (XAFS) measurements [20] under the same experimental conditions ($H = 2$ T). The Ge $K$-edge XAFS is very sensitive to the bond-breaking transition due to the dramatic change in Ge-Ge(Si) distances connecting the Gd slabs ($\approx 1$ Å) [8]. This is especially the case for the $x = 0.125$ sample, where the transition between two orthorhombic ($O$) polymorphs involves breaking of all slab-connecting Ge(Si)-Ge(Si) bonds, whereas half of the slabs remain connected at the $O$ to monoclinic ($M$) transition for $x = 0.5$ [3,13] (FM order occurs *only* when *all* slabs are connected). The sudden loss of XAFS intensity in the low-$R$ region of the spectra containing Ge-Ge(Si) pair correlations [arrow in Fig. 2(a)] is one of the signatures of the bond-breaking transition which, on warming, is centered at 80 K and 270 K for $x = 0.125, 0.5$ samples, respectively [vertical lines in Fig. 1(c)]. XAFS modeling using the known crystal structures [8,13,21] confirms the nature of the transition. For example, the slab-connecting Ge-Ge(Si) bonds change from a bonding distance of 2.67(1) Å to a nonbonding distance of 3.62(1) Å for $x = 0.125$. The modeling uses FEFF6.0 standards [22], a weighted average of contributions from the three inequivalent Ge sites, and a random occupation of Ge/Si sites [8,23].
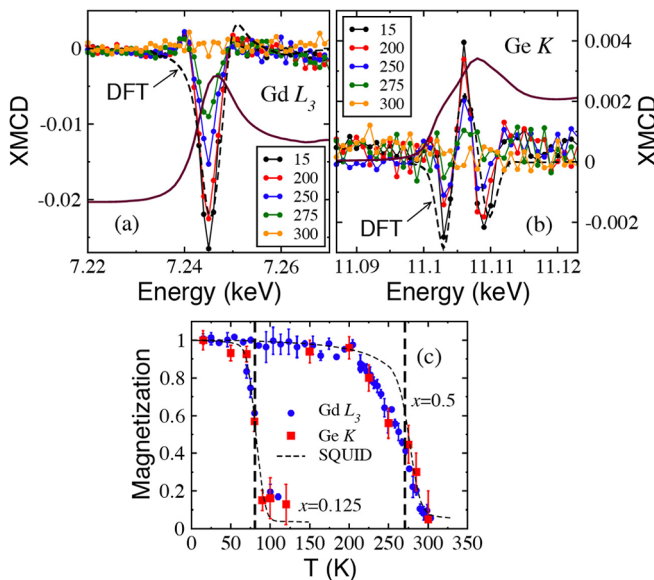


FIG. 1 (color online). Top panel: Gd $L_3$ and Ge $K$ edge-jump normalized XMCD data for $x = 0.5$ at $H = 2$ T. The helicity-independent absorption coefficient (scaled to fit) is shown with solid lines. Results from DFT calculations are superimposed (dashed lines). At this field XMCD is half its saturation value, and calculations were scaled accordingly. Lower panel: temperature dependence of Ge and Gd XMCD signals together with SQUID bulk-magnetization data ($H = 2$ T) for $x = 0.125, 0.5$ samples. Vertical dashed lines indicate the centroids of the bond-breaking structural transition.
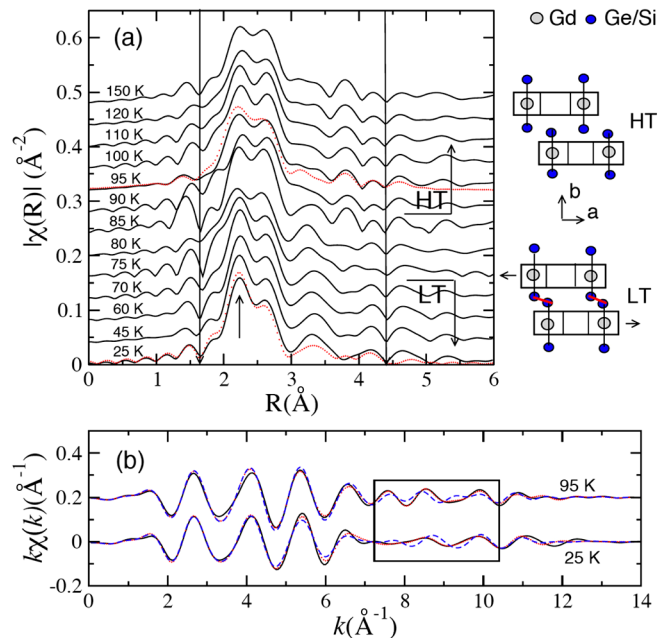


FIG. 2 (color online). Far right: schematic of the structure showing slab-connecting Ge(Si)-Ge(Si) bonds. Gd also occupies sites at the slabs' edges and Ge(Si) also occupies sites near the center of the slabs [3]. (a) Magnitude of complex Fourier transform (FT) of Ge $K$-edge XAFS data in the $k = [2, 13]$ Å$^{-1}$ range for $x = 0.125$ (lines) and representative fits (points) using the known low temperature (LT) and high temperature (HT) crystal structures [21]. $k$ is photoelectron wave number. Peaks in the FT are shifted toward shorter distances by $\approx 0.35$ Å due to photo-electron scattering phase shifts. Vertical lines delimit the fitted region with corresponding back-Fourier transformed data and fits shown in (b). A large misfit is obtained when short (long) bonds are forced to be present in HT (LT) phases (dashed lines).

To gain insight into the origin of induced magnetic polarization in Ge and to assess the importance of RKKY interactions in mediating interslab magnetic coupling, we carried out full potential linearized augmented plane wave (LAPW) calculations using the local density approximation approach with Gd $4f$ electrons treated as core states [24]. The calculations were performed using the $x = 0.5$ crystal structure [13] with Ge atoms occupying the slab-connecting sites ($T'$ sites in Ref. [13] and labeled $Ge_{1,2}$ in Fig. 3) and Si atoms occupying intraslab sites. The $Ge_{1,2}$ sites are equivalent in the $O$ phase but are inequivalent in the $M$ phase where every second slab is shifted. The calculations are for $T = 0$ K, with FM order imposed on both structures in order to investigate the link with magnetism. The calculations do find the FM $O$ phase lower in total energy than the FM $M$ phase (experimentally, FM order is only found in the $O$ phase). We note that full occupation of $T'$ sites by Si yields insignificant changes in Gd magnetism in the $O$ phase [9]. Experimentally, occupation of Ge/Si sites is nearly random [13].

Figure 3 shows spin-density contour maps (left panel) arising from states between $-1.5$ eV and the Fermi level (0 eV) for each structure. This energy region is where the most dramatic changes occur in the electronic structure as a result of the structural transition. The important Ge $4p$ and Gd $5d$ projected density of states (DOS) are shown in the right panel of Fig. 3 for slab-connecting $Ge_2$ sites and the nearest Gd sites at the slab's edge (Gd2 and Gd2B sites in Ref. [13] for $O$ and $M$ phases, respectively). There are much smaller changes in the unoccupied states above the Fermi level. Indeed, the total charge inside each muffin-tin sphere changes little, indicating that most rearrangements of wave functions and energy levels occur among the occupied states. For example, the average Gd $5d$ charge is 1.27 (1.24) electrons in the $O$ ($M$) structure. The average

spin moment on the $5d$ orbitals, however, changes from $0.41\mu_B$ in the $O$ phase to $0.29\mu_B$ in the $M$ phase. The DOS plots clearly demonstrate a strong spin-dependent hybridization between Ge $4p$ and Gd $5d$ states. The stronger hybridization for spin-down states is due to Gd $5d$ spin-down states being more extended (spin-up states are lower in energy because of their exchange interaction with the occupied $4f$ orbitals) [25]. This hybridization is the basis for the observed induced polarization at Ge sites. The good agreement between calculated and measured XMCD at Gd $L_3$ and Ge $K$ edges (Fig. 1), even for such subtle polarization on Ge $4p$ states at $T'$ sites ($S_z = -0.033\mu_B$, $L_z = -0.00025\mu_B$), validates the electronic structure calculations in the $O$ phase [26]. Since $K$-edge XMCD is proportional to $d\langle L_z \rangle/dE$, with $\langle L_z \rangle$ the orbital moment in Ge $4p$ states [27], Fig. 1(b) indicates a significant variation in the orbital polarization of Ge $4p$ states with energy, but an integrated orbital moment near zero, in agreement with the calculations.

The Ge-Ge bond-breaking accompanying the slabs' shear displacement is the primary structural change and the cause of the dramatic changes in the spin density and DOS shown in Fig. 3. The intraslab distances change little [3], and the same is true for the spin density within the slabs. The Ge-Ge bond between the slabs is quite strong in the $O$ structure, only about 10% longer than in elemental Ge (diamond structure). The $4p$ charge density halfway between the bonded Ge atoms is 0.051 $e/a_0^3$ compared to 0.074 $e/a_0^3$ for pure Ge ($a_0$ is Bohr radius). In the $M$ structure the charge density is 0.019 $e/a_0^3$ as a result of the weakened bond.

To confidently relate the significant changes in electronic structure to the FM ordering of $4f$ moments we evaluated the changes expected in the RKKY interslab $4f$-$4f$ exchange coupling. This coupling arises from the
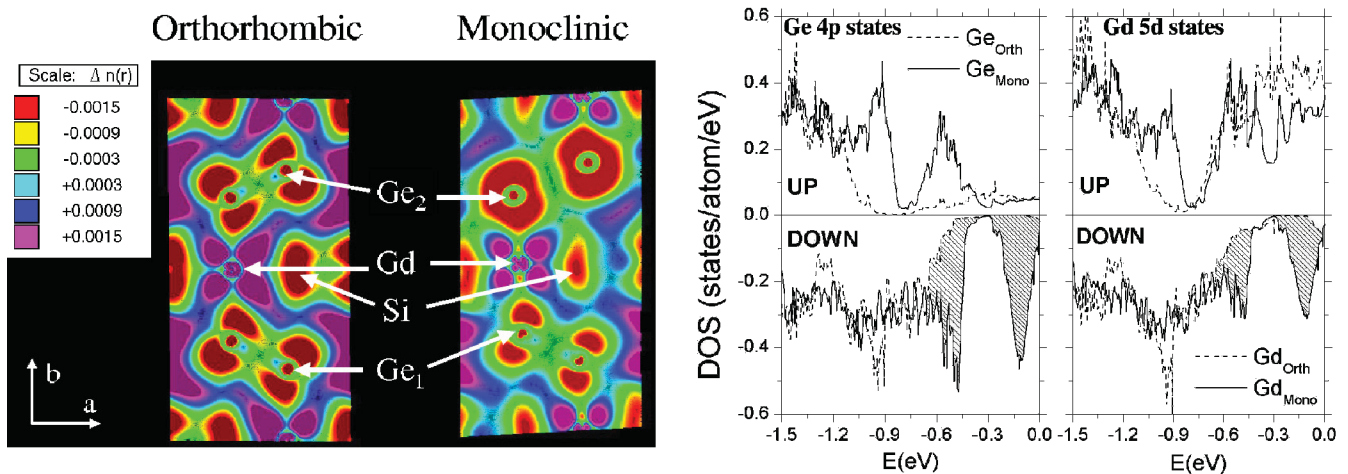


FIG. 3 (color).   Left panel: spin-density contour plots of the $(a, b, 0.5)$ plane for $O$ and $M$ structures ($x = 0.5$). The atoms are slightly off the plane (about 0.28 Å for $Ge_2$ in the $M$ structure). The distance between $Ge_2$ atoms is about 2.6 Å and 3.5 Å in $O$ and $M$ structures, respectively. The spin density (in $e/a_0^3$ units, $a_0$ Bohr radius) includes states extending from $-1.5$ eV to 0 eV ($E_F$). Right panel: projected density of $4p$ states at bond-breaking $Ge_2$ sites and $5d$ states on the nearest Gd site at the slab's edge ($\sim$2.5 Å off the plane in contour plots). Hatched regions show the spin-down states that develop in the $M$ structure.

PHYSICAL REVIEW LETTERS

conduction band wave functions having an exchange interaction with the local $4f$ moments. Since the $5d$ component of the wave function has the largest exchange interaction with the $4f$ electrons [25], the relative strength of FM exchange coupling between Gd atoms at sites $i$ and $j$ can be evaluated using $J_{ij}(q = 0) \propto \sum_k \langle P_{5d_i}\psi_k | P_{5d_j}\psi_k \rangle$, where $\psi_k$ are conduction band wave functions, $P_{5d_i}\psi_k$ their $5d$ component on site $i$, $q = 0$ the wave vector for FM order, and the sum is over states near the Fermi level. It can be seen that if a wave function is to contribute to the $4f$-$4f$ exchange coupling it must have significant Gd-$5d$ components on *both* site $i$ and site $j$. If $i$ and $j$ are on neighboring slabs, then the $5d$-$4p$ hybridization allows the Ge-Ge link between the slabs to facilitate hybridized wave functions with enhanced Gd-$5d$ components on both sites. Direct $5d$-$5d$ overlap between sites in neighboring slabs, on the other hand, is negligible. We used the expression above to estimate the relative strengths of intermoment coupling in the two structures. We find that the $J_{ij}$ for pairs of Gd atoms across disconnected slabs are ~20% reduced compared to the $J_{ij}$ for pairs across connected slabs. The $J_{ij}$ for pairs of Gd atoms within the slabs are much less affected by the structural transition. The results not only explain the disappearance of FM order at the bond-breaking transition, but also help understand the emergence of FM order in $Gd_5Ge_4$ when interslab, Ge-Ge bonds are formed upon the application of magnetic fields [8] or high pressures [28].

In summary, the spin-dependent hybridization between Ge $4p$ and Gd $5d$ conduction states in $Gd_5(Ge_{1-x}Si_x)_4$ alloys is modified by the bond-breaking magnetostructural transition reducing the net Gd $5d$ moment and the strength of FM RKKY exchange coupling across sheared slabs. The magnetic polarization at Ge sites is rooted in this hybridization and the agreement between XMCD experiment and theory validates our description of magnetization density, albeit only in the $O$ FM state. The results highlight the delicate interplay between structure and magnetism which is at the core of the magnetocaloric effect displayed by this important class of materials.

[1] V. K. Pecharsky and K. A. Gschneidner, Jr., Phys. Rev. Lett. **78**, 4494 (1997).

[2] L. Morellon *et al.*, Phys. Rev. B **58**, R14721 (1998); **62**, 1022 (2000).

[3] V. K. Pecharsky and K. A. Gschneidner, Jr., Adv. Mater. **13**, 683 (2001).

[4] B. N. Harmon and V. N. Antonov, J. Appl. Phys. **93**, 4678 (2003).

[5] F. Casanova *et al.*, Eur. Phys. J. B **40**, 427 (2004).

[6] F.-J. Peres-Reche *et al.*, Phys. Rev. B **73**, 014110 (2006).

[7] J. D. Moore *et al.*, Phys. Rev. B **73**, 144426 (2006).

[8] V. K. Pecharsky, A. P. Holm, K. A. Gschneidner, Jr., and R. Rink, Phys. Rev. Lett. **91**, 197204 (2003).

[9] D. Paudyal, Phys. Rev. B **73**, 144406 (2006).

[10] H. Tang *et al.*, Phys. Rev. Lett. **93**, 237203 (2004).

[11] M. A. Ruderman and C. Kittel, Phys. Rev. **96**, 99 (1954); T. Kasuya, Prog. Theor. Phys. **16**, 45 (1956); K. Yosida, Phys. Rev. **106**, 893 (1957).

[12] V. K. Pecharsky and K. A. Gschneidner, Jr., J. Alloys Compd. **260**, 98 (1997).

[13] W. Choe *et al.*, Phys. Rev. Lett. **84**, 4617 (2000).

[14] G. Schütz *et al.*, Phys. Rev. Lett. **58**, 737 (1987); P. Carra and M. Altarelli, Phys. Rev. Lett. **64**, 1286 (1990); J. Stöhr, J. Magn. Magn. Mater. **200**, 470 (1999).

[15] P. W. Anderson, Phys. Rev. B **79**, 350 (1950).

[16] K. Hirano, K. Izumi, T. Ishikawa, S. Annaka, and S. Kikuta, Jpn. J. Appl. Phys. **30**, L407 (1991); J. C. Lang and G. Srajer, Rev. Sci. Instrum. **66**, 1540 (1995).

[17] Two 400 $\mu$m-thick diamond (111) crystals were oscillated in tandem (synchronized to ~2 msec), each at the $\lambda/8$ wave-plate condition ($\pi/4$ phase shifter). This doubles the angular offset $\Delta\theta$ needed to produce circular light relative to a single phase plate at the $\lambda/4$ condition, reducing systematic errors at the relatively high Ge $K$-edge energy ($\Delta\theta \sim E^{-3}$). At the lower energy Gd $L_3$ edge, only one crystal was used at the $\lambda/4$ condition.

[18] Both samples have the same $O$ ($Pnma$) crystal structure in the FM state. Si doping contracts the lattice enhancing $T_c$.

[19] H. Sakurai *et al.*, J. Phys. Soc. Jpn. **62**, 459 (1993); G. Schütz *et al.*, Phys. Rev. Lett. **58**, 737 (1987).

[20] E. A. Stern, Phys. Rev. B **10**, 3027 (1974); P. A. Lee and J. B. Pendry, Phys. Rev. B **11**, 2795 (1975).

[21] Note that the low- and high-$T$ orthorhombic polymorphs correspond to the high- and low-$H$ phases, respectively, induced in $Gd_5Ge_4$ by an applied magnetic field [8].

[22] S. Zabinsky, J. J. Rehr, A. Ankudinov, R. C. Albers, and M. J. Eller, Phys. Rev. B **52**, 2995 (1995).

[23] The limited information in the powder-averaged, multi-sited XAFS data prevented us from quantifying deviations from random Ge or Si occupancies.

[24] B. N. Harmon *et al.*, J. Phys. Chem. Solids **56**, 1521 (1995).

[25] B. N. Harmon and A. J. Freeman, Phys. Rev. B **10**, 4849 (1974).

[26] XMCD averages over all three Ge inequivalent sites, with $T'$ sites accounting for half of all Ge atoms.

[27] H. Ebert in *Spin-Orbit Influenced Spectroscopies*, edited by H. Ebert and G. Schütz (Springer, New York, 1996), p. 160.

[28] C. Magen *et al.*, Phys. Rev. Lett. **91**, 207202 (2003).